nature cell biology

Genome-wide RNA-mediated interference screen identifies miR-19 targets in Notch-induced T-cell acute lymphoblastic leukaemia

Konstantinos J. Mavrakis[1,12], Andrew L. Wolfe[1,2,12], Elisa Oricchio[1], Teresa Palomero[3,4], Kim de Keersmaecker[4], Katherine McJunkin[5,6], Johannes Zuber[5], Taneisha James[5,11], Kenneth Chang[5], Aly A. Khan[2,7], Christina S. Leslie[7], Joel S. Parker[8], Patrick J. Paddison[9], Wayne Tam[10], Adolfo Ferrando[3,4] and Hans-Guido Wendel[1,13]

MicroRNAs (miRNAs) have emerged as novel cancer genes. In particular, the miR-17–92 cluster, containing six individual miRNAs, is highly expressed in haematopoietic cancers and promotes lymphomagenesis *in vivo*. Clinical use of these findings hinges on isolating the oncogenic activity within the 17–92 cluster and defining its relevant target genes. Here we show that miR-19 is sufficient to promote leukaemogenesis in *Notch1*-induced T-cell acute lymphoblastic leukaemia (T-ALL) *in vivo*. In concord with the pathogenic importance of this interaction in T-ALL, we report a novel translocation that targets the 17–92 cluster and coincides with a second rearrangement that activates *Notch1*. To identify the miR-19 targets responsible for its oncogenic action, we conducted a large-scale short hairpin RNA screen for genes whose knockdown can phenocopy miR-19. Strikingly, the results of this screen were enriched for miR-19 target genes, and include *Bim* (*Bcl2L11*), AMP-activated kinase (*Prkaa1*) and the phosphatases *Pten* and *PP2A* (*Ppp2r5e*). Hence, an unbiased, functional genomics approach reveals a coordinate clampdown on several regulators of phosphatidylinositol-3-OH kinase-related survival signals by the leukaemogenic miR-19.

miRNAs are ubiquitous regulators of biological processes involved in normal development, differentiation, and diseases including cancer. They act by regulating gene expression at the transcriptional and translational levels[1]. Several methods have been devised to identify genes that are regulated by miRNAs; programs such as Targetscan can identify potential miRNA targets on the basis of conserved sequence complementarity[2–4]. Experimental tools can define the actual effects of miRNAs on gene expression, for example expression profiles and comparative proteomics (stable isotope labelling with amino acids in cell culture; SILAC)[5,6], or measurements of incorporation into the miRNA machinery (high-throughput sequencing of RNAs isolated by crosslinking immunoprecipitation; HITS-CLIP)[7]. These approaches are capable of predicting or identifying a large number of miRNA target genes; however, most probably only a limited number of miRNA targets are directly responsible for a specific phenotype[8]. An unbiased way of identifying these functionally relevant miRNA targets is needed for an understanding of the biological basis of miRNA activity.

The oncogenic 17–92 cluster of miRNAs is of eminent importance in human haematopoietic cancers[9–11]. Overexpression of the 17–92 cluster produces a benign lymphoproliferation and can cooperate with c-*Myc* in causing Burkitt's lymphoma in mice[9,10]. The cluster has two paralogues and together they encode 15 miRNAs with overlapping functions in development[12]. miR-19 is clearly important in cooperating with c-*Myc* or enhancing the transplantation of Burkitt's lymphoma cells[13,14]; however, it has not been established which particular miRNA(s) deliver the oncogenic activity of these clusters in leukaemia. Moreover, although comprehensive lists of potential targets of the 17–92 cluster are available, and some individual candidates have been confirmed experimentally[12,15,16], the mechanism responsible for its oncogenicity remains unknown.

RESULTS

Distinct role of miR-19 in lymphocyte survival and transformation

To identify the oncogenic activity within the 17–92 cluster and its paralogues we used an *in vitro* assay of haematopoietic transformation[17]. We

[1]Cancer Biology & Genetics Program, Memorial Sloan-Kettering Cancer Center, 1275 York Avenue, New York, New York 10021, USA. [2]Weill Cornell Graduate School of Medical Science, New York, New York 10065, USA. [3]Department of Pathology, [4]Institute for Cancer Genetics, Columbia University, New York, New York 10032, USA. [5]Cold Spring Harbor Laboratory, Cold Spring Harbor, New York 11724, USA. [6]Watson School of Biological Sciences, Cold Spring Harbor Laboratory, Cold Spring Harbor, New York 11724, USA. [7]Computational Biology, Memorial Sloan-Kettering Cancer Center, New York, New York 10021, USA. [8]Expression Analysis Inc., Durham, North Carolina 27502, USA. [9]Fred Hutchinson Cancer Research Center, Seattle, Washington 98109, USA. [10]Department of Pathology and Laboratory Medicine, Joan and Sanford I. Weill Medical College of Cornell University, New York, New York 10025, USA. [11]Present address: Department of Gene and Cell Medicine & Black Family Stem Cell Institute, Mount Sinai School of Medicine, New York, New York 10029, USA.
[12]These authors contributed equally to this work.
[13]Correspondence should be addressed to H.-G.W. (e-mail: wendelh@mskcc.org)

Received 7 December 2009; accepted 5 February 2010; published online 28 February 2010; DOI:10.1038/ncb2037

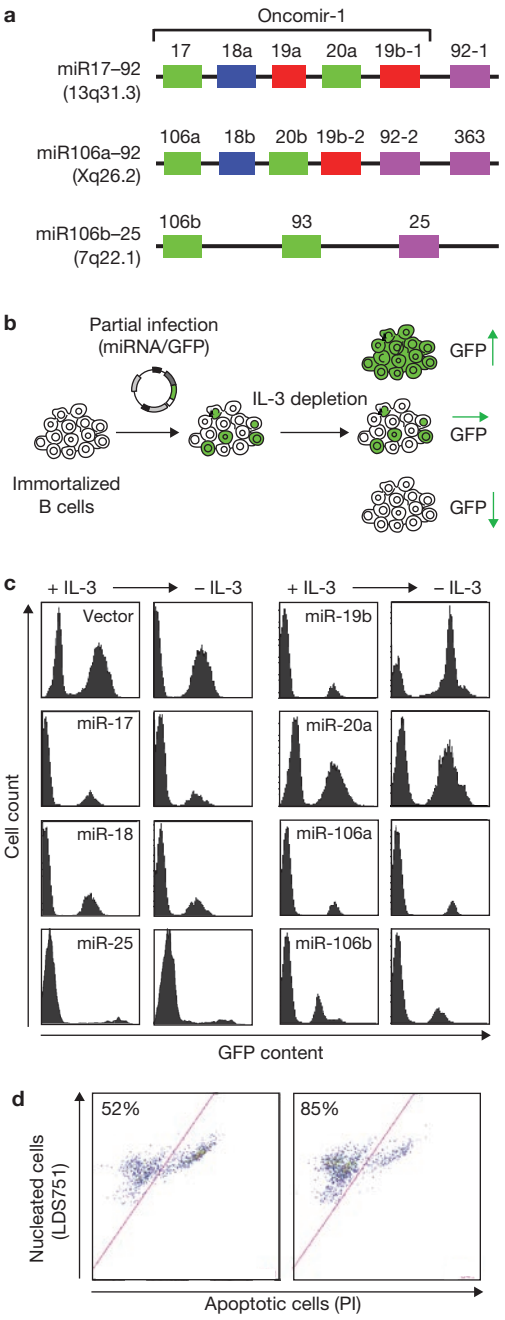

Figure 1 miR-19 enhances cytokine independent survival *in vitro*. (**a**) Genomic organization of the 17–92 cluster (including 'oncomir-1') and its paralogues; miRNAs shown in identical colour share common seed sequences. (**b**) Diagram of the competition assay for cytokine-independent survival of immortalized FL5-12 lymphocytes. (**c**) Representative FACS profiles showing enrichment of miR-19/GFP-expressing FL5-12 cells on depletion of IL-3, whereas populations transduced with vector or the other miRNAs remain unchanged (all experiments were conducted in triplicate). +IL-3 and –IL-3 indicate the presence or absence of IL-3. (**d**) Representative FACS profiles measuring cell viability in FL5-12/vector cells (left) in comparison with FL5-12/miR-19 (right). The percentage of viable cells after 36 h of IL-3 depletion is indicated.

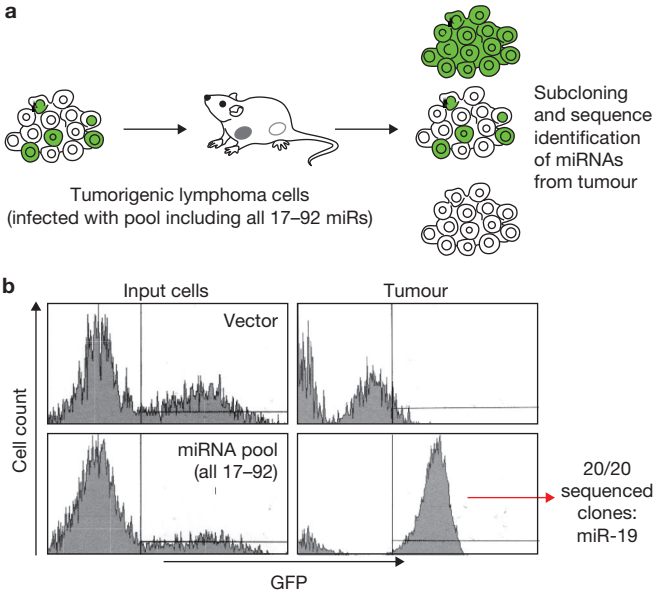

Figure 2 Pooled miRNA screen for tumorigenic activities within the 17–92 cluster and its paralogues. (**a**) Diagram of experimental design for a retroviral, pooled miRNA tumorigenicity screen *in vivo*. (**b**) Histograms for GFP distribution in tumorigenic Myc-transgenic lymphocytes and resultant tumours for cells infected with empty vector or pooled miRNAs encoded in the 17–92 cluster and its paralogues. Tumour DNA was isolated and the integrated miRNA(s) were amplified by PCR and subcloned; 20 clones were picked for sequence identification of the integrated miRNA. Sequencing revealed that all 20 clones harboured the miR-19 vector.

tested all miRNAs representing families of seed sequences, specifically miR-17, miR-18a, miR-19b-1 (miR-19), miR-20a, miR-106a, miR-106b and miR-25 (Fig. 1a)[12]. The assay is based on the interleukin-3 (IL-3) dependence of FL5-12 lymphocytes, which undergo apoptosis when removed from IL-3. We partly transduced FL5-12 cells with the individual miRNAs and green fluorescent protein (GFP) or empty vector (MIG), and monitored these mixed populations by fluorescence-activated cell sorting (FACS) for changes in their relative proportions (Fig. 1b). FL5-12 cells expressing miR-19 were rapidly enriched over parental cells after depletion of IL-3, and none of the other miRNAs had a similar protective effect (Fig. 1c) (miR-19, $P < 0.002$; all other miRNAs and vector, $P > 0.05$; t-test). Next, we determined whether the effect was due to a decrease in cell death or to an effect on proliferation. miR-19 showed direct protection from cell death in FL5-12 cells after withdrawal of IL-3 (FL5-12/vector, viability 49 ± 1% (mean ± s.d.)); FL5-12/miR-19, viability 82 ± 1.5%; $P < 6 \times 10^{-6}$) (Fig. 1d). By contrast, miR-19 had little effect on cell proliferation, such that 24 h after release the fraction of synchronized FL5-12 cells in S phase was indistinguishable between vector-transduced and miR-19-transduced cells (FL5-12/vector, 24 ± 3%; FL5-12/miR-19, 24.5 ± 0.5%; $P = 0.8$) (not shown). Hence, miR-19 has a distinct ability within the 17–92 cluster to protect lymphocytes from apoptosis after depletion of growth factors.

The 17–92 cluster of miRNAs has been studied extensively in a murine model of Burkitt's lymphoma[10,13,14]. To confirm the dominant role of miR-19 in that model, we transduced lymphoma cells with a pool of miRNAs that included all 17–92 members. We then transplanted these cells into non-irradiated recipient mice and sequenced the integrated miRNA vectors from the resulting tumours (Fig. 2a). As expected, we found a marked enrichment of miRNA/GFP-expressing cells. Strikingly, all sequences (20 out of 20 clones) derived from the tumour identified the miR-19 construct (Fig. 2b). Consistent with its ability to block apoptosis *in vitro* was our observation that miR-19 was also sufficient to prevent *p53* loss of heterozygosity (LOH) in tumours derived from $p53^{+/-}$/*Myc* haematopoietic progenitors (HPCs),

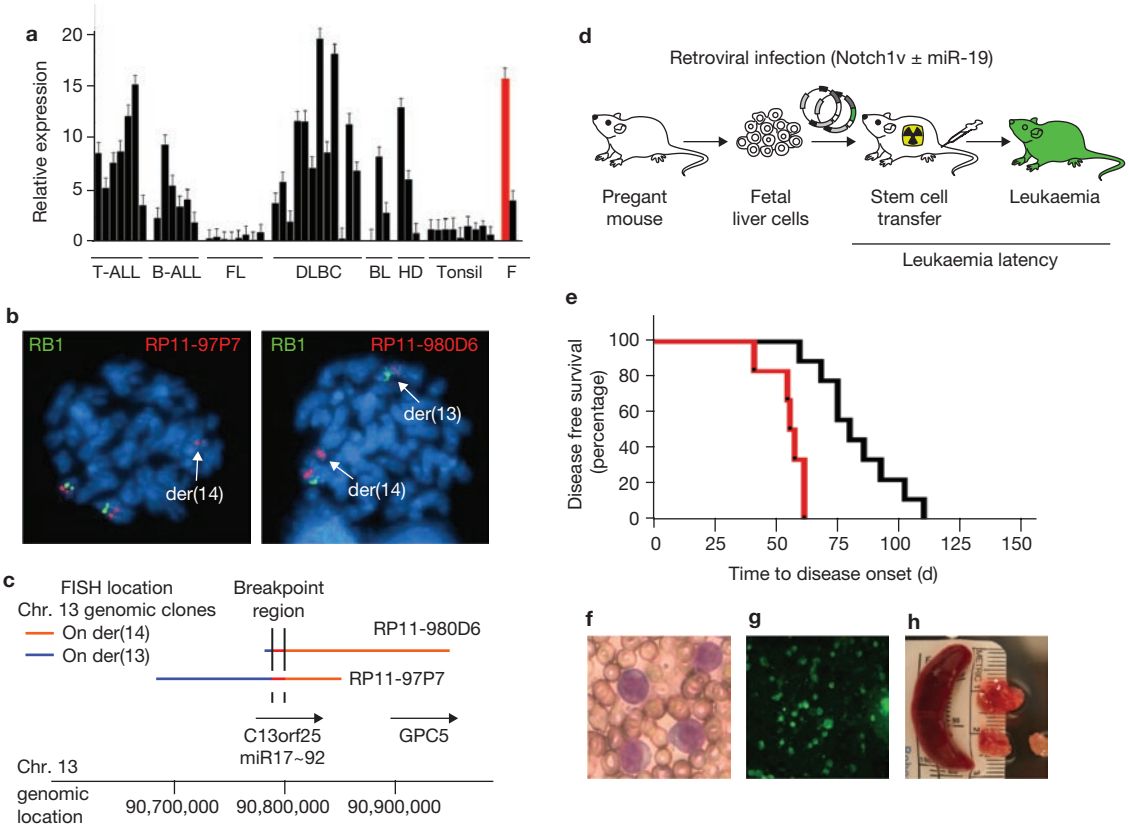

Figure 3 miR-19 is a novel T-ALL oncogene. (**a**) Quantitative RT–PCR measurement of miR-19 expression in a panel of human lymphoid malignancies. T-/B-ALL, T-cell and B-cell acute lymphoblastic leukaemia; FL, follicular lymphoma; DLBC, diffuse large B-cell lymphoma; BL, Burkitt's lymphoma; HD, Hodgkin's disease; tonsil, lymphocytes from reactive tonsils; F, FL5-12 cells, both parental (black bar) and miR-19 transduced (red bar). Results are shown as means and s.d. (**b**) Double-colour fluorescence *in situ* hybridization (FISH) analysis of t(13;14)(q32;q11) with an RB1 probe (green) in 13q14 and genomic clones RP11-97P7 and RP11-980D6 overlapping the 17–92 locus in 13q32 (red). (**c**) Graphic representation of FISH results. Chr., chromosome. (**d**) Mouse model of *Notch1*-induced T-ALL. (**e**) Kaplan–Meier analysis of leukaemia-free survival after HPC transplantation. Red, Notch-ICN + miR-19 ($n = 6$); black, Notch-ICN + vector ($n = 9$). (**f**–**h**) Representative photomicrographs of *Notch1*/miR-19-induced ALL. (**f**) Leukaemic blasts on blood film. (**g**) Effacement of the bone marrow by miR-19/GFP-expressing leukaemic cells. (**h**) Splenomegaly and lymphomas. The pathological appearance of *Notch*1-induced leukaemia is identical (not shown).

which inevitably undergo *p53* LOH in vector controls (Supplementary Information, Fig. S1). Clearly, miR-19 is sufficient to affect lymphocyte survival and transformation *in vitro* and *in vivo*.

miR-19 is a novel oncogene in acute T-ALL

We assessed the expression of miR-19 in a panel of human lymphatic malignancies to determine its relevance in these cancers. In comparison with lymphocytes from tonsils, we found a 5–17-fold increased expression of miR-19 in T-ALL ($n = 3$) (Fig. 3a; Supplementary Information, Table S1). Moreover, miR-19 showed the highest expression of all miRNAs encoded in the 17–92 cluster in this disease (Supplementary Information, Fig. S2a). miR-19 was also highly expressed in B-cell acute lymphoblastic leukaemia (B-ALL) and aggressive lymphomas including diffuse large B-cell lymphoma and Burkitt's disease. In concord with previous profiling studies[18,19], we found lower levels in indolent follicular lymphomas. The retroviral expression of miR-19 in FL5-12 cells produced levels that were comparable to those seen in some tumour and leukaemia specimens (red bar in Fig. 3a).

The 17–92 cluster is the target of a novel translocation in T-ALL. Karyotype analysis of an adult patient with T-ALL revealed the coexistence of two clonal translocations involving both TCRA/D loci in chromosome band 14q11. The first rearrangement, t(9;14)(q34;q11), affects the *NOTCH1* gene locus in chromosome band 9q34, and 5′ rapid amplification of cDNA ends confirmed the expression of a constitutively active form of *NOTCH1* (exons 29–34) (Supplementary Information, Fig. S2b–d)[20,21]. The second rearrangement, t(13;14)(q32;q11), also involving the TCRA/D locus, was novel and pinpointed a new T-ALL oncogene at 13q32. A fluorescence *in situ* hybridization analysis using genomic clones RP11-980D6 and RP11-97P7 revealed a split signal between chromosome 13 and the derivative chromosome 14, and mapped the breakpoint close to the 17–92 cluster t(13;14)(q32;q11) (Fig. 3b, c; Supplementary Information, Fig. S2e). Thus, dual translocations that simultaneously affect the 17–92 cluster and *Notch1* indicate the oncogenic importance of this interaction in T-ALL.

Indeed, most cases of T-ALL show mutations or translocations that result in increased expression or constitutive *Notch1* activity[20–22]. To determine whether miR-19 could enhance *Notch1*-induced T-ALL *in vivo*, we co-transduced HPCs from fetal livers with Notch-ICN (intracellular cleaved Notch1) and miR-19 or empty vector[23]. We then transplanted the HPCs into irradiated recipients and monitored them for the onset of frank leukaemia (Fig. 3d). Mice receiving HPCs expressing both Notch-ICN and miR-19 succumbed to ALL in about 2 months. At the same time, 80% of the mice receiving Notch-ICN remained healthy ($P = 0.0003$) (Fig. 3e). Pathology confirmed the diagnosis of T-ALL with

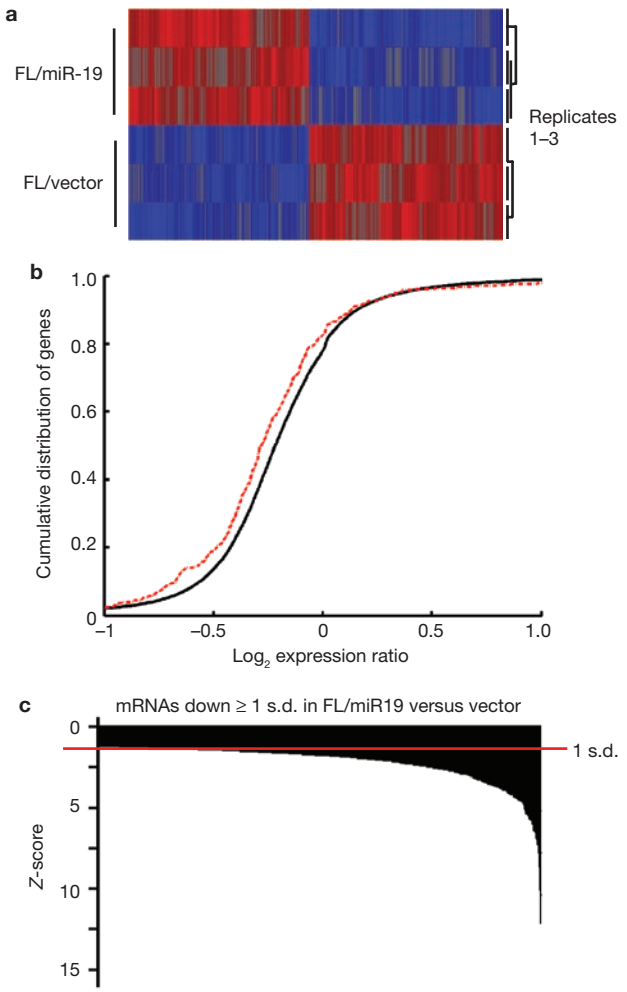

Figure 4 Gene expression analysis of parental and miR-19-transduced FL5-12 cells. (**a**) Heat-map illustration of the unsupervised clustering analysis reveals differences in gene expression between parental (FL/vector) and miR-19-expressing FL5-12 cells (FL/miR-19). (**b**) Comparison of the change in expression of predicted miR-19 targets represented on the array (336 genes, red line) versus all represented genes (8,065 genes, black line) ($P < 2 \times 10^{-4}$; Kolmogorov–Smirnov test). (**c**) Histogram of genes whose expression is downregulated by more than 1 s.d. in FL5-12/miR-19 cells in comparison with parental cells: miR-19 target genes are not over-represented among genes showing more pronounced (1.5 or 2 SD) decreases in expression. An expression array readily detects global downregulation by miR-19 but is not a sufficient filter to define key miR-19 targets.

abundant lymphoblasts, marrow infiltration, splenomegaly, and isolated lymphomas (Fig. 3f–h; Supplementary Information, Fig. S3a–e). The blasts showed expression of T-cell markers Thy-1, CD4 and CD8, in the absence of other lineage markers (Supplementary Information, Fig. S3f, and Supplementary Information, Table S2). Leukaemia arising in animals that received HPCs transduced with *Notch1* alone were pathologically indistinguishable (not shown). Hence, miR-19 cooperates with *Notch-1* in a murine model of T-ALL.

Target prediction and expression analyses show global effects on miR-19 target genes

We now wished to determine which molecular targets were responsible for the oncogenicity of miR-19. Initially we combined computational target identification and gene expression analyses. Targetscan predicted 938 human and 744 murine miR-19 targets (Supplementary Information, Tables S3 and S4). Gene expression profiles in FL5-12 cells transduced with miR-19 or vector showed only modest changes in expression (mean fold change -0.2 ± 0.39 (mean ± s.d.)) (Fig. 4a). Overall, expression levels of all predicted miR-19 targets were decreased more than those for other genes ($P < 2 \times 10^{-4}$; Kolmogorov–Smirnov test) (Fig. 4b). Among these were also potentially interesting candidates such as the *Pten* tumour suppressor. However, there was no significant enrichment of miR-19 targets among genes showing more pronounced (1.5 or 2 s.d.) decreases in expression ($P > 0.46$ at 2 s.d.; $P > 0.077$ at 1.5 s.d.; Fisher's exact test) (Fig. 4c; Supplementary Information, Table S5). Thus, expression analysis and target prediction readily confirm global effects of miR-19 and may lead to promising candidates, but they do not provide strong enough filters to identify the most relevant miR-19 targets.

Genetic screens can pinpoint functionally relevant miRNA target genes

We wondered whether an unbiased genetic screen might be an alternative method for the functional identification of miR-19 targets involved in lymphocyte survival. Specifically, we reasoned that a short hairpin RNA (shRNA) screen[25,26] for genes whose knockdown phenocopied miR-19 in lymphocytes should also identify the genes responsible for miR-19 action. We conducted extensive control experiments with increasing dilutions of miR-19 and also a shRNA against *Bim* (*Bcl2L11*), a known target of the 17–92 cluster[9,10] (Supplementary Information, Fig. S4a–d). We then devised a screening protocol involving transduction of FL5-12 cells with pools of about 1,000 shRNAs, and two cycles of IL-3 depletion or continued passage in complete medium (Fig. 5a). We used custom half-hairpin arrays to measure changes in the abundance of shRNAs in treated (without IL-3) versus untreated (including IL-3) samples at two time points (t_1 and t_2 equal one or two cycles of IL-3 depletion, respectively)[27]. Unsupervised clustering showed good reproducibility between biological replicates (A–C; correlation coefficient $r = 0.60 \pm 0.17$; mean ± s.d.), and revealed a progressive shift in shRNAs across subsequent cycles of IL-3 depletion (Fig. 5b). Statistical tools helped us to identify biologically significant signals. A significance analysis of microarrays (SAM) identified changes in individual shRNAs (Fig. 5c; see Supplementary Information, Table S6, for the full analysis). A gene set analysis (GSA) defined groups of shRNAs targeting the same genes. The GSA identified 14 genes, each targeted by at least two and up to five different shRNAs, and the top 'hit' was the α subunit of AMP-activated kinase (*Prkaa1*) targeted by five independent shRNAs (Fig. 5d; see Supplementary Information, Table S7, for the full analysis).

We individually validated candidate genes in the same experimental system. We included nearly all genes identified from the GSA, and also tested protein-coding genes from the SAM above an arbitrary threshold (at least 1.65-fold increase; $P < 0.05$). In total, we retested more than 70 genes and typically three shRNAs against each (all genes included in the validation are highlighted in Supplementary Information, Tables S6 and S7). Ultimately, shRNAs against eight genes positively validated and produced a survival benefit in FL5-12 cells depleted of IL-3 (in triplicate experiments P (vector/not shown) > 0.2; P (for all shRNAs) < 0.05; t-test) (Fig. 5e). The positive validation rate was about 10%, and this may reflect the lower stringency of the SAM, which included genes targeted by just one shRNA.

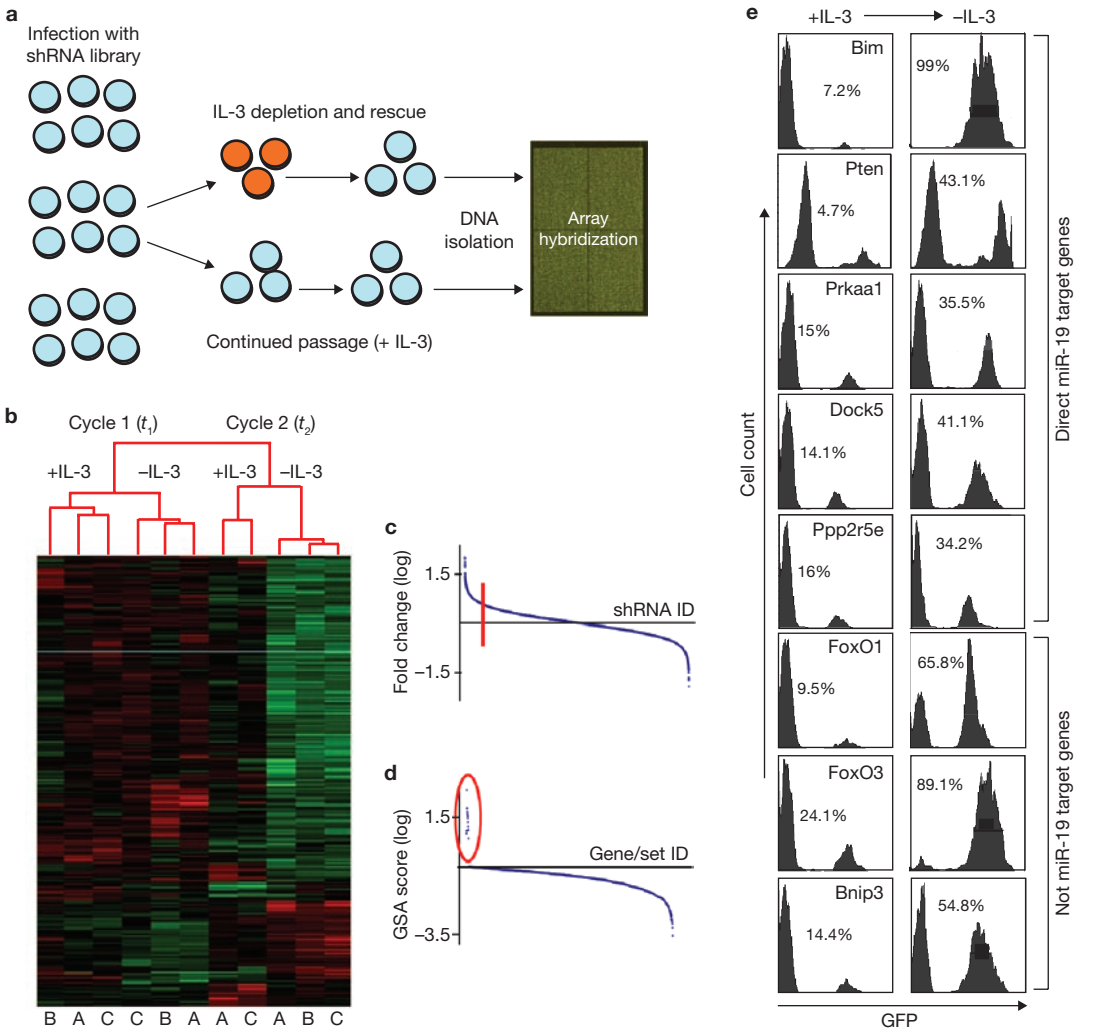

Figure 5 Genetic screen for shRNAs that phenocopy miR-19 in lymphocyte survival. (**a**) Design diagram of the pooled shRNA screen, in which large populations of FL5-12 cells are transduced with library pools and subjected to IL-3 depletion. (**b**) Heat map of the unsupervised clustering analysis of the half-hairpin array results. t_1, t_2, time points after 1 and 2 cycles of IL-3 depletion; –IL-3, treated group; +IL-3, untreated group; A–C, replicates (replicate B at t_2/+IL-3 was removed for technical reasons). (**c**) SAM data indicating fold change ($\log_2$) for individual shRNAs and the threshold for validation studies (red line). (**d**) GSA identifies enrichment of sets of shRNAs targeting 14 genes (red circle). (**e**) Representative FACS profiles from triplicate validation experiments showing the enrichment of FL5-12 cells expressing the indicated shRNAs and GFP after depletion of IL-3. Vector alone showed no change (not shown).

Strikingly, in the human genome five of the eight validated 'hits' harboured binding sequences for miR-19. Besides the pro-apoptotic *Bim*[9], these were the tumour suppressor gene *Pten*[9] and the genes encoding the α subunit of AMP-activated kinase (*Prkaa1*), the ε isoform of PP2A (*Ppp2r5e*), and dedicator of cytokinesis-5 (*Dock5*). In addition, we validated three other genes that did not contain miR-19-binding sites in their 3′ untranslated regions (UTRs), namely those encoding the FoxO transcription factors *FoxO1* and *FoxO3*, and *Bnip3*, a regulator of Rheb/mTOR and Bcl2-binding protein. Taken together, the results of this unbiased genetic screen for shRNAs that behave like miR-19 showed a highly significant enrichment for genes containing miR-19-binding sites ($P < 7.2 \times 10^{-7}$ by Fisher's exact test; Fig. 6a). Unlike the human *DOCK5* gene, the mouse gene is not a miR-19 target, and calculation of the enrichment statistics for the murine genome confirmed similarly high significance levels ($P < 3.2 \times 10^{-5}$ by Fisher's exact test; Fig. 6b). The prediction of miR-19 sites is based on Targetscan and did not take into account potential non-classical miRNA-binding sites, for example those in the coding sequence. However, some of the eight genes also harbour potential coding-sequence sites; these are shown in Supplementary Information, Table S13. Thus, our unbiased, large-scale shRNA screen identified five human and four murine genes whose knockdown phenocopied miR-19 action in lymphocyte survival and that harboured miR-19-binding sites in their 3′ UTRs.

miR-19 acts through a coordinate effect on several negative regulators of phosphatidylinositol-3-OH kinase signals

We now wished to test whether miR-19 actually regulates the expression of these genes. Reporter assays confirmed direct 3′ UTR inhibition mediated by the predicted binding sites for these genes ($n = 3$) (Fig. 7a; Supplementary Information, Tables S9 and S12). We used quantitative RT–PCR to measure the effect of miR-19 on mRNA levels of *Pten*, *Ppp2r5e*, *Prkaa1* and *Bim* in miR-19-expressing murine T-ALL cells (Supplementary

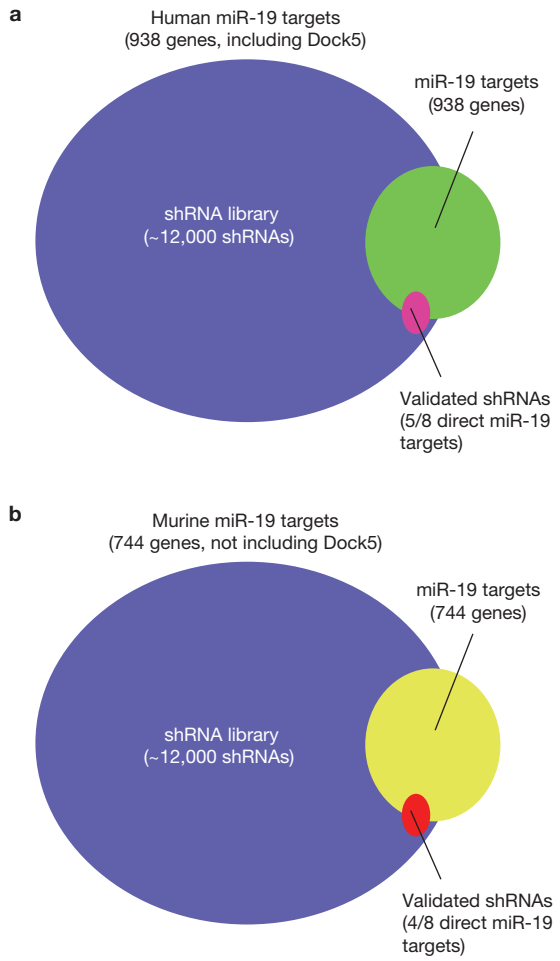

Figure 6 Summary of the screen result. (**a**) Beginning with a genome-scale shRNA library of ~12,000 shRNAs and 7,853 unique targets, only shRNAs against eight genes validated positively, and five of these contained a miR-19 seed match, compared with 938 predicted miR-19 targets. Hence, the genetic screen results in a highly significant enrichment for miR-19 target genes ($P < 7.2 \times 10^{-7}$; Fisher's exact test). (**b**) Identical analysis for the murine genome, which contains 744 predicted miR-19 target genes, and where the murine Dock5 gene is not a target. Fisher's exact test confirms enrichment for miR-19 targets in the murine genome ($P < 3.2 \times 10^{-5}$). Predictions are based on Targetscan 4.2; validation is based on individual testing of three shRNAs per gene, positively validated implies survival benefit in FL5-12 cells ($P < 0.05$).

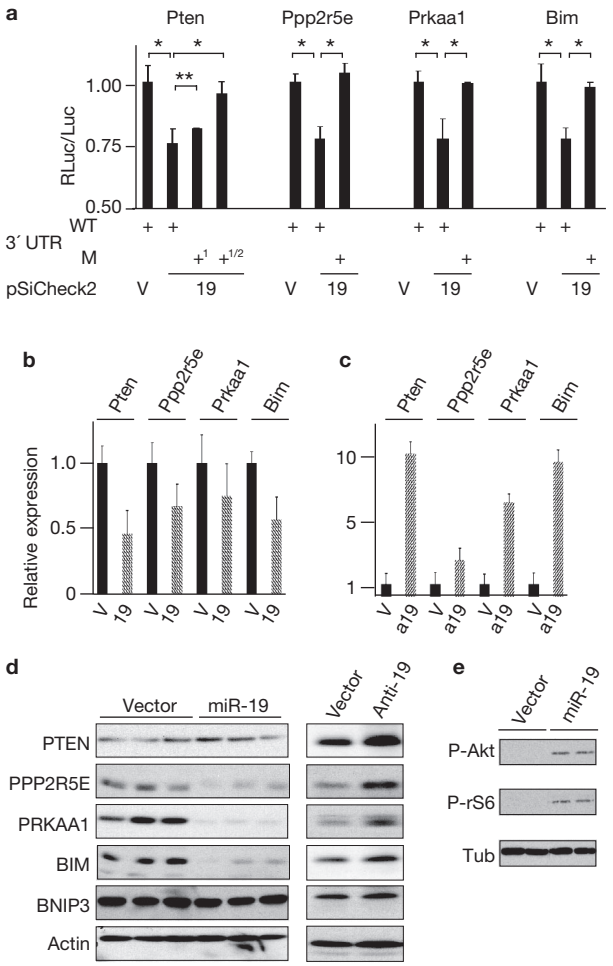

Figure 7 The identified genes are actual targets of miR-19. (**a**) Reporter assay for 3′ UTR repression by miR-19. Inhibition of the 3′ UTR by miR-19 is indicated as the ratio of *Renilla* luciferase to firefly luciferase activity (RLuc/Luc); means and s.d. are shown. WT, wild-type 3′ UTR; M, 3′ UTR in which the miR-19 binding site has been mutated; for Pten one site ($+^{1}$) or both sites ($+^{1/2}$) were mutated. Significance: asterisk, $P < 0.05$; two asterisks, $P > 0.05$. (**b**) Quantitative RT–PCR (qRT–PCR) for the indicated genes on cDNA prepared from vector (V, black bars) or miR-19-transduced (19, shaded bars) FL5-12 cells. Expression levels (means and s.d.) are normalized to the vector controls (relative expression). (**c**) qRT–PCR comparing FL5-12 cells transduced with vector (V, black bars) and antagomirs to miR-19 (a19, shaded bars) analysed as above. (**d**, **e**) Immunoblots on lysates from vector, miR-19 or antagomir (Anti-19)-transduced FL5-12 cells probed for the indicated proteins (see also Supplementary Information, Fig. S6). Uncropped images of blots are shown in Supplementary Information, Fig. S8.

Information, Fig. S5a, b) and also in FL5-12 cells (Fig. 7b), in which we consistently observed up to twofold decreases ($n = 3$; P (vector vs. miR-19) < 0.05 for all four genes; *t*-test) (Supplementary Information, Table S8). Conversely, an antagomir against miR-19 caused an increase in mRNA levels *in vitro* ($n = 3$; P (vector versus anti-19) < 0.05 for all four genes) (Fig. 7c; Supplementary Information, Table S8), and both miR-19 and the antagomir had measurable effects on protein levels. For example, miR-19 produced a clear decrease in PPP2R5E, PRKAA1 and BIM, and resulted in overall activation of phosphatidylinositol-3-OH kinase (PI(3)K) signalling, as indicated by increased phosphorylation of Akt and the ribosomal S6 protein (Fig. 7d, e), whereas we did not detect an effect of miR-19 on PTEN protein, its mRNA was clearly decreased, and the antagomir produced increases in all miR-19 target proteins including PTEN (Fig. 7c, d). As expected, neither miR-19 nor the antagomir had an effect on *Bnip3*, which does not contain a 3′ UTR site for miR-19 (Fig. 7d). The larger effects of the antagomir in comparison with miR-19 expression may indicate that these genes are tonically suppressed by the endogenous miR-19 in proliferating cells. Hence, we confirm that the expression of *Bim*, *Pten*[9], *Prkaa1* and *Ppp2r5e* is regulated by miR-19 in lymphocytes.

Next, we wondered about the contribution of these multiple target genes to miR-19 action. The pro-apoptotic BIM protein opposes Bcl2 and is an important regulator of lymphocyte survival[28]. To measure whether miR-19 had effects independent of *Bim*, we conducted complementation studies with FL5-12 cells engineered to stably express *Bcl2* (FL5-12/*Bcl2* cells). As expected, the *Bim* shRNA conferred no additional benefit, whereas miR-19 and the shRNAs against *Pten* and *Pp2r5e* showed continued enrichment

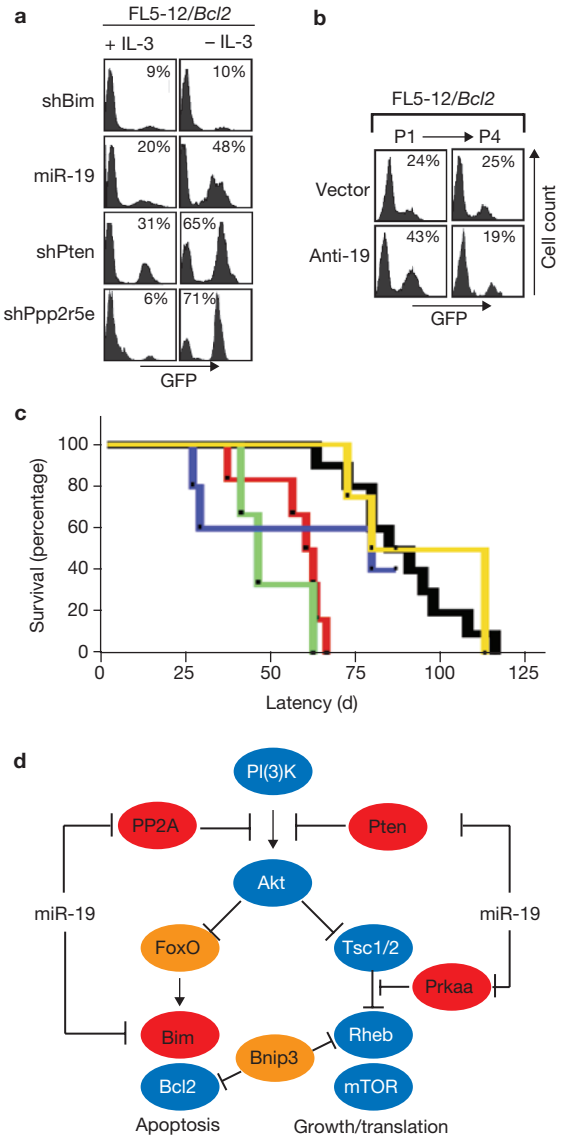

Figure 8 miR-19 acts through multiple negative regulators of PI(3)K-related survival signals. (**a**) Representative FACS profiles of triplicate experiments on FL5-12 cells co-expressing Bcl2 (FL5-12/*Bcl2*) and the indicated shRNAs or miR-19 and GFP. Cells were shifted from complete (+IL-3) to IL-3-deficient (–IL-3) medium to assess *Bcl2*-independent effects on lymphocyte survival. (**b**) FACS analysis of FL5-12/*Bcl2* cells transduced with antagomir (Anti-19) or vector and GFP, and grown in complete medium. (**c**) *In vivo* knockdown of individual target genes accelerates *Notch1*-induced T-ALL *in vivo*. A Kaplan–Meier analysis of survival after HPC transplantation is shown. Black, vector ($n = 10$); green, shPten ($n = 4$); red, shBim ($n = 6$); blue, shPrkaa ($n = 5$); yellow, shPp2r5e ($n = 4$). (**d**) Diagram indicating the multilevel control of PI(3)K survival signals by miR-19.

in the presence of *Bcl2* (Fig. 8a). Conversely, an antagomir against miR-19 produced anti-proliferative effects, and FL5-12/*Bcl2* cells expressing the antagomir were lost on continued passage (Fig. 8b). Similarly, miR-19 maintained its protective effect in the presence of metformin-activated AMP kinase or enforced expression of *Pten* or *Pp2r5e* (Supplementary Information, Fig. S5c). This indicates that multiple target genes contribute to miR-19 action *in vitro*. *In vivo* we found that individual knockdown of some targets was sufficient to accelerate leukaemogenesis. This was most striking for *Pten* ($n = 4$, vector $n = 10$; $P < 0.001$) and *Bim* ($n = 6$; $P < 0.001$), whereas shRNA against *Prkaa1* produced a modest effect ($n = 5$; $P = 0.3$), and knockdown of *Pp2r5e* alone was unable to drive leukaemogenesis ($n = 4$) (Fig. 8c). Overall our data identify multiple miR-19 targets that together act on PI(3)K-related signals and affect lymphocyte survival *in vitro* and leukaemogenesis *in vivo* (Fig. 8d).

DISCUSSION

Our results provide new insights into the oncogenic activity of the miR-17–92 cluster in T-cell leukaemia. miR-19, expressed at levels seen in human tumours, enhances lymphocyte survival and can promote *c-Myc*-induced B-cell lymphomagenesis[13,14]. Moreover, miR-19 is sufficient to cooperate with *Notch1* in T-ALL *in vivo*. Given the conservation of the entire 17–92 cluster, it is likely that these miRNAs perform important functions in other tissues or biological processes, or that the co-expression of these miRNAs produces additional effects[11]. The interaction of *Notch1* and miR-19 is a relevant pathogenic mechanism in T-ALL. This is most strikingly demonstrated by the coexistence in the same leukaemic clone of two translocations activating the *NOTCH1* gene (t(9;14)(q34;q11)) and targeting the 17–92 cluster (t(13;14)(q32;q11)), respectively. It is likely that other mechanisms, for example transcriptional activation by *c-Myc* and *Notch1*, are more common causes of the increased miR-19 expression that we observed in T-ALL specimens. Clearly, miR-19 is an important oncogene within the 17–92 cluster and contributes to the molecular pathogenesis of lymphoma and T-cell leukaemia.

We have identified a pattern of gene regulation by miR-19. Using an unbiased shRNA screening approach we have found eight genes whose knockdown recapitulates miR-19 effects *in vitro*. Intriguingly, in the human genome, five of these 'hits' harbour miR-19-binding sites and are regulated by miR-19. It is likely that these genes are among the key effectors of miR-19 action in lymphocyte survival and that the regulation of multiple genes contributes to the overall activity of miR-19. These include *Bim*, encoding a pro-apoptotic *Bcl2* protein and target of the 17–92 cluster[12], and also *Prkaa1* (encoding AMP-activated kinase), the tumour suppressor phosphatases *Pp2a* (subunit *Ppp2r5e*) and *Pten*[8] (Fig. 8d). A candidate gene approach combining the analysis of predicted miR-19 targets and expression data has also pointed to Pten in a mouse lymphoma model[13,14]. Other miRNAs encoded in the 17–92 cluster are predicted to target some of the same genes, suggesting a potential mechanism for the functional cooperation between these clustered miRNAs[8]. These results suggest that miR-19 coordinates a PI(3)K-pathway-related program of cell survival in lymphocytes that contributes to leukaemogenesis.

Our results validate a new functional genomics approach for identifying miRNA target genes. A genetic screen provides an unbiased tool with which to pinpoint miRNA target genes that may be responsible for a specific phenotype, such as lymphocyte survival. Some limitations should be noted, for example that shRNAs and miRNAs act through somewhat distinct mechanisms[3,29]. Further, our screen is based on shRNAs that target single genes whose individual knockdown is sufficient to recapitulate the effect of miR-19. It is likely that these genes are among the key effectors of miR-19. However, we may overlook weaker targets whose effect is apparent only in the context of additional expression changes. shRNA and screens are an evolving technology, and limitations of detection and shRNA validation may account for the overall low (10%) validation rate. Despite these limitations, our data indicate that phenotype-based genetic screens provide an unbiased tool with which to pinpoint functionally important miRNA targets.

In this manner, genetic screens can complement computational[4,30] and genomic/proteomic[5,7] methods in deciphering the complexity of gene regulation by miRNAs. □

METHODS

Methods and any associated references are available in the online version of the paper at http://www.nature.com/naturecellbiology/

Note: Supplementary Information is available on the Nature Cell Biology website.

ACKNOWLEDGEMENTS

We thank Lin He, S. W. Lowe and G. Hannon for access to shRNA and miRNA screening technologies; W. Pear, J. Huse and E. C. Holland for plasmids; H. Zhu for technical assistance; the Memorial Sloan-Kettering (MSK) animal facility and Research Animal Resource Center (RARC), A. Viale of the MSK Genomics Core, H. Zhao of the cBIO program, and J. Schatz and J. Massagué for editorial advice; and V. Murty for cytogenetic and fluorescence *in situ* hybridization analyses. This work was supported by grants from the American Cancer Society, the Geoffrey Beene Cancer Center, the Leukemia Research Foundation, the Louis V. Gerstner Foundation, the May and Samuel Rudin Foundation, the NY Community Trust and the William and Blanche Foundation (to H.-G.W.), from the Andrew Seligson Memorial Clinical Fellowship (to J.Z.), and NYStar (to P.J.P.). A.F. is supported by R01CA120196, the WOLF Foundation, the Rally across America Foundation and the Leukemia and Lymphoma Society (grants 1287-08 and 6237-08), and A.F. is a Leukemia & Lymphoma Society Scholar.

AUTHOR CONTRIBUTIONS

K.J.M, A.L.W. and E.O. performed experimental design and analysis. K.d.K., T.P. and A.F. conducted T-ALL translocation analysis. K.M., J.Z., T.J. and K.C. performed the screen and analysis. A.A.K., C.S.L. and J.S.P. did data analysis. P.J.P. generated the shRNA library. W.T. was responsible for clinical specimens. H.-G.W. designed the study and wrote the paper.

COMPETING FINANCIAL INTERESTS

The authors declare no competing financial interests.

Published online at http://www.nature.com/naturecellbiology
Reprints and permissions information is available online at http://npg.nature.com/reprintsandpermissions/

1 Bartel, D. P. MicroRNAs: genomics, biogenesis, mechanism, and function. *Cell* **116,** 281–297 (2004).
2 Friedman, R. C., Farh, K. K., Burge, C. B. & Bartel, D. P. Most mammalian mRNAs are conserved targets of microRNAs. *Genome Res.* **19,** 92–105 (2009).
3 Grimson, A. *et al.* MicroRNA targeting specificity in mammals: determinants beyond seed pairing. *Mol. Cell* **27,** 91–105 (2007).
4 Lewis, B. P., Shih, I. H., Jones-Rhoades, M. W., Bartel, D. P. & Burge, C. B. Prediction of mammalian microRNA targets. *Cell* **115,** 787–798 (2003).
5 Baek, D. *et al.* The impact of microRNAs on protein output. *Nature* **455,** 64–71 (2008).
6 Selbach, M. *et al.* Widespread changes in protein synthesis induced by microRNAs. *Nature* **455,** 58–63 (2008).
7 Chi, S. W., Zang, J. B., Mele, A. & Darnell, R. B. Argonaute HITS-CLIP decodes microRNA–mRNA interaction maps. *Nature* **460,** 479–486 (2009).
8 Xiao, C. & Rajewsky, K. MicroRNA control in the immune system: basic principles. *Cell* **136,** 26–36 (2009).
9 Xiao, C. *et al.* Lymphoproliferative disease and autoimmunity in mice with increased miR-17–92 expression in lymphocytes. *Nature Immunol.* **9,** 405–414 (2008).
10 He, L. *et al.* A microRNA polycistron as a potential human oncogene. *Nature* **435,** 828–833 (2005).
11 Mendell, J. T. miRiad roles for the miR-17–92 cluster in development and disease. *Cell* **133,** 217–222 (2008).
12 Ventura, A. *et al.* Targeted deletion reveals essential and overlapping functions of the miR-17 through 92 family of miRNA clusters. *Cell* **132,** 875–886 (2008).
13 Mu, P. *et al.* Genetic dissection of the miR-17~92 cluster of microRNAs in Myc-induced B-cell lymphomas. *Genes Dev.* **23,** 2806–2811 (2009).
14 Olive, V. *et al.* miR-19 is a key oncogenic component of mir-17–92. *Genes Dev.* **23,** 2839–2849 (2009).
15 O'Donnell, K. A., Wentzel, E. A., Zeller, K. I., Dang, C. V. & Mendell, J. T. c-Myc-regulated microRNAs modulate E2F1 expression. *Nature* **435,** 839–843 (2005).
16 Petrocca, F. *et al.* E2F1-regulated microRNAs impair TGFβ-dependent cell-cycle arrest and apoptosis in gastric cancer. *Cancer Cell* **13,** 272–286 (2008).
17 Plas, D. R., Talapatra, S., Edinger, A. L., Rathmell, J. C. & Thompson, C. B. Akt and Bcl-xL promote growth factor-independent survival through distinct effects on mitochondrial physiology. *J. Biol. Chem.* **276,** 12041–12048 (2001).
18 Malumbres, R. *et al.* Differentiation stage-specific expression of microRNAs in B lymphocytes and diffuse large B-cell lymphomas. *Blood* **113,** 3754–3764 (2009).
19 Calin, G. A. & Croce, C. M. Investigation of microRNA alterations in leukemias and lymphomas. *Methods Enzymol.* **427,** 193–213 (2007).
20 Palomero, T. *et al.* Activating mutations in NOTCH1 in acute myeloid leukemia and lineage switch leukemias. *Leukemia* **20,** 1963–1966 (2006).
21 Ellisen, L. W. *et al.* TAN-1, the human homolog of the *Drosophila* notch gene, is broken by chromosomal translocations in T lymphoblastic neoplasms. *Cell* **66,** 649–661 (1991).
22 Weng, A. P. *et al.* Activating mutations of NOTCH1 in human T cell acute lymphoblastic leukemia. *Science* **306,** 269–271 (2004).
23 Pear, W. S. *et al.* Exclusive development of T cell neoplasms in mice transplanted with bone marrow expressing activated Notch alleles. *J. Exp. Med.* **183,** 2283–2291 (1996).
24 Edgar, R., Domrachev, M. & Lash, A. E. Gene Expression Omnibus: NCBI gene expression and hybridization array data repository. *Nucleic Acids Res.* **30,** 207–210 (2002).
25 Paddison, P. J. *et al.* A resource for large-scale RNA-interference-based screens in mammals. *Nature* **428,** 427–431 (2004).
26 Silva, J. M. *et al.* Profiling essential genes in human mammary cells by multiplex RNAi screening. *Science* **319,** 617–620 (2008).
27 Chang, K., Elledge, S. J. & Hannon, G. J. Lessons from Nature: microRNA-based shRNA libraries. *Nature Methods* **3,** 707–714 (2006).
28 Bouillet, P. *et al.* Proapoptotic Bcl-2 relative Bim required for certain apoptotic responses, leukocyte homeostasis, and to preclude autoimmunity. *Science* **286,** 1735–1738 (1999).
29 Paddison, P. J., Caudy, A. A., Sachidanandam, R. & Hannon, G. J. Short hairpin activated gene silencing in mammalian cells. *Methods Mol. Biol.* **265,** 85–100 (2004).
30 John, B. *et al.* Human microRNA targets. *PLoS Biol.* **2,** e363 (2004).

DOI: 10.1038/ncb2037

METHODS

Cell culture, viability, proliferation assays and vector constructs. FL5-12 murine lymphocytes, cell cycle, apoptosis studies and viral transductions were as described[17,31]. All vectors are based on murine stem cell virus, and include the miRNA expression vector encoding miR17, miR18a, miR19b-1 (miR-19), miR106a, miR106b miR25 (ref. 10), Notch-ICN (a gift from W. Pear)[23], *Bcl2* (ref. 32) and the individual shRNA vectors (protein knockdown by shRNAs (Supplementary Information, Fig. S6) and vector constructs (Supplementary Information, Fig. S7a, b, and Supplementary Information, Table S10)). The miRNA pool contained 48 miRNAs (all 17–92 and additional control miRNAs; the complete list is available from the authors on request). Expression of 17–92 miRs in FL5-12 cells is shown in Supplementary Information, Fig. S7c. The antagomirs MZIP19a-PA-1, MZIP19b-PA-1 and scrambled control (MZIP000-PA-1) were from System Biosciences (Supplementary Information, Fig. S7d).

Generation of mice. The mouse T-ALL and EμMyc lymphoma models have been reported[23,32]. Data were analysed in Kaplan–Meier format with the log-rank (Mantel–Cox) test for statistical significance. The *p53* LOH PCR and surface marker analysis were as described[32].

Western blot analysis. Immunoblots were performed from whole-cell lysates as described[32]. Antibodies were against Prkaa1 (2532, 1:1,000 dilution; Cell Signaling), Bim/Bcl2L11 (AAP-330, 1:1,000; Assay Designs), FoxO1 (94545, 1:1,000; Cell Signaling), FoxO3a (9467, 1:1,000; Cell Signaling), phospho-FoxO3a (94665, 1:1,000; Cell Signaling), Ppp2r5e (NB 100-845; Novus), Pten (9559, 1:1,000; Cell Signaling), tubulin (B-5-1-2, 1:5,000; Sigma), actin (AC-15, 1:5,000; Sigma), Bnip3 (3769, 1:1,000; Cell Signaling), phosphorylated S6 (2215, 1:1,000; Cell Signaling) and phosphorylated Akt (4058, 1:1,000; Cell Signaling). The Dock5 antibody was a gift from Alan Hall (Memorial Sloan-Kettering Cancer Center).

Real-time quantitative PCR. Total RNA and miRNA-enriched RNA were extracted with the Allprep DNA/RNA/Protein (Qiagen) and miRNeasy Mini (Qiagen) kits. Pathological diagnosis was by expert haematopathologists at Weill Cornell University. cDNA synthesis and qRT–PCR and analysis by the $\Delta\Delta C_t$ method as described[31]. Taqman Gene Expression Assays: Bcl2l11 (Mm00437796_m1), Dock5 (Mm00555757_m1), FoxO1 (Mm00490672_m1), FoxO3 (Mm01185722_m1), Ppp2r5e (Mm00803759_m1), Prkaa1 (Mm01296695_m1), Pten (Mm01212532_m1), mouse GAPD (GAPDH; 4352932; Applied Biosystems) and miR-19b (000396, Applied Biosystems) expression was normalized to RNU6B (001093; Applied Biosystems); primer sequences for miRNA detection are available from the authors on request.

Luciferase assays. The Dock5, Ppp2r5e, Prkaa1 and Bim 3′-UTR fragments (Supplementary Information, Table S11) were generated by PCR and cloned into the psi-CHECK-2 vector (Promega). The assays were performed as described[9]. The binding-site mutants were generated by site-directed mutagenesis (Supplementary Information, Table S12).

Karyotype and fluorescence *in situ* hybridization (FISH) analysis. Metaphase chromosome preparations made from primary lymphoblasts from patients were subjected to karyotype analysis by following standard procedures. Genomic clones RP11-97P7 and RP11-980D6 located at 13q32 were from Invitrogen. DNA was labelled by nick-translation with spectrum orange dUTP fluorochrome (Vysis). A spectrum-green-labelled RB1 probe was used as control for chromosome 13q hybridization. FISH was performed by standard methods on cells used for cytogenetic analysis. Hybridization signals were scored on at least 20 metaphase spreads on 4,6-diamidino-2-phenylindole-stained slides, with the Cytovision Imaging system attached to a Nikon Eclipse 600 microscope (Applied Imaging).

Amplification of aberrant *NOTCH1* transcripts by 5′ rapid amplification of cDNA ends (RACE). mRNA was extracted from primary lymphoblasts from patients by using the Nucleotrap mRNA extraction kit from Clontech, and 5′ RACE was performed with the SMART RACE kit (Clontech) by using a oligonucleotide primer complementary to the sequence of exon 29 of the *NOTCH1* gene (5′-TCGTCCATGAGGGCACCGTCTGAAG-3′).

Pooled shRNA library screen. The pooled shRNA screen and half-hairpin array detection has been described; the library has been cloned from the original PSM2 constructs into the MRP vector and it contains about 14,000 distinct shRNAs, pooled into 1,000 shRNAs per pool[26,27,31]. FL5-12 cells were transduced at low multiplicity of infection in triplicates and each was subjected to two cycles of IL-3 depletion and rescue (t_1 and t_2). Samples were collected after viability had recovered for DNA isolation, PCR amplification of integrated shRNAs or the library as a reference; these were labelled and hybridized. Data generated (Nimblescan software) from image scans (Axon 4000BScanner) were imported into R version 2.4 for processing and analysis. Each Nimblegen 12-plex custom array consists of 12,033 half-hairpin probes (sequences are available from the authors on request). Most were represented by shRNAs in the library, and the remainder were used for background estimation. Negative control spots showed lower intensities than the experimental probes on each array (Supplementary Information, Fig. S7e). Signal values below background were replaced with the background estimate to dampen large ratios resulting from low signal. The two channels for each array were then normalized with loess normalization, and log ratios of the normalized intensity were used in further analyses.

Data analysis for pooled shRNA screens. The analyses were performed with the Bioconductor linear models for microarray (limma)[33], SAM[34] and GSA[35] libraries in R. Correlations between biological replicates were calculated for each time point, and principal component analyses were performed to determine the magnitude of experimental effects and biological replicates. Biological replicates did not constitute a major source of variation in the experiment. The mean correlation for biological replicates was 0.60 ± 0.17 s.d., and probably reflected random variations as populations drifted in culture. Biologically significant signals were identified with the SAM software to select probes reflecting differences in relative abundance of shRNAs. We used the unpaired two-class algorithm, which assumes independent samples of each feature across the conditions. *Q* values are calculated empirically and used for identifying significant features. Overall, a gene was scored as being a potential candidate if its shRNA probe was found to fulfil these criteria: at least 1.65-fold change, $P < 0.05$, and current gene bank annotation with a corresponding protein. Further testing was performed with GSA to identify candidates based on data from multiple hairpins targeting the same gene; because each gene is targeted by two to four hairpins, their fold changes are summed. This statistic was compared with the same statistic from exhaustive permutation to arrive at empirical *P* values for each gene. All gene sets showing a positive fold change in the GSA were included in validations (except olfactory receptor481). These cutoffs are relatively arbitrary and were chosen as a conservative criterion to minimize false positives.

Computational analysis of shRNA off-target effects. We performed several computational analyses to investigate whether the results of the screen might be attributable to off-target effects. We considered two hypotheses: first, that shRNAs over-represented in the screen have a sequence similarity to miR-19 itself and hence mimic miR-19 activity through sites in 3′ UTRs; and second, that results of the screen are explainable by microRNA-like off-target effects on a few key genes. We ranked all shRNAs by ungapped sequence similarity of, on the one hand, the shRNA 'seed' (positions 2–8) to the miR-19 seed region and, on the other hand, the shRNA to the full-length miR-19a and miR-19b sequences. No shRNAs in the library had the same heptamer seed region as miR-19; among the shRNAs whose seed region matched the miR-19 heptamer seed at six positions (12 shRNAs with hexamer seeds matching positions 3–8, two shRNAs with hexamer seeds matching positions 2–7), none were in the top 100 shRNAs over-represented in the screen. The maximal sequence similarity between shRNAs in the library and the full-length miR-19a/b sequences was a 13-base ungapped match; 23 shRNAs had this degree of similarity to miR-19a and/or miR-19b, but none of them occurred in the top 100 over-represented shRNAs from the screen. Moreover, we found poor Spearman rank correlation ($|\rho| < 0.01$) between the ranking of shRNAs by over-representation in the screen and these similarity comparisons to miR-19. Next, we considered whether shRNAs that were highly ranked in the screen were more likely to have predicted off-target effects on *Pten*, *Prkaa1*, *Bcl2l11*, *Ppp2r5e, Dock5, Foxo1, Foxo3 And Bnip3*, compared with the full library. If this were true, over-representation of an shRNA in the screen might be explainable through off-target silencing of these key genes. To predict potential microRNA-like off-target effects of shRNAs, we scanned 3′ UTRs in the entire mouse genome for matches to heptamer seed sequences (positions 2-8, no conservation filter) of shRNAs in the library. A gene with a heptamer seed match for a given shRNA was considered to be a predicted off-target for this shRNA. We

then tested whether, for any of the eight genes, the set of shRNAs that were predicted to 'off-target' the gene were enriched in the top K over-represented shRNAs from the screen, in comparison with the full shRNA library. We used values of K ranging from 2 to 250, and we did not observe statistical significance by a Fisher's exact test for any value of K ($P > 0.05$ in all cases for each gene). These controls indicate that the shRNAs are not similar to miR-19 itself and that the screen result could not be explained by off-target effects of top-ranked shRNAs on key genes. We computed the enrichment statistic with respect to the number of unique targets of the roughly 12,000 shRNAs in the library and the subset of these targets that were also predicted miR-19 targets; we used Fisher's exact test to account for the small number of 'hits'. This analysis was performed for both the human and the murine genome. Target predictions were as defined in Targetscan 5.1.

Expression array analysis. RNA isolation, quality control, cRNA synthesis, labelling hybridization and scanning were performed in accordance with standard protocols and the manufacturer's instructions (Affymetrix) and analysed with Partek Genomic Suite 6.4. For statistical analysis, we centred the data with the mean $\log_2$(expression change) of genes and normalized them to have unit variance in $\log_2$(expression change) across all genes. This normalization results in a modified Z-transformation of the data (Z-score). These data have been deposited in NCBI's Gene Expression Omnibus[24] under GEO accession number GSE20097 (http://www.ncbi.nlm.nih.gov/geo/query/acc.cgi?acc=GSE20097).

Kolmogorov–Smirnov (KS) statistic. To compare the expression changes for miR-19 targets with those for all genes, we compared their distributions of log(expression change) values by using a one-sided KS statistic, which assesses whether the distribution of expression changes for one set is significantly shifted downwards (downregulated) compared with the distribution for the other set. The KS statistic computes the maximum difference in value of the empirical cumulative distribution functions:

$$\sup_x (F_1(x) - F_2(x))$$

where $F_j(x) = \frac{1}{n_j} \sum_{i=1}^{n_j} I_{X_i \le x}$ is the empirical cumulative distribution function for gene set $j = 1, 2, \ldots$ based on nj (Z-transformed) log(expression change) values. We used the Matlab function kstest2 to calculate the KS test statistic and asymptotic P value.

31 Mavrakis, K. J. *et al*. Tumorigenic activity and therapeutic inhibition of Rheb GTPase. *Genes Dev.* **22,** 2178–2188 (2008).
32 Wendel, H. G. *et al*. Survival signalling by Akt and eIF4E in oncogenesis and cancer therapy. *Nature* **428,** 332–337 (2004).
33 Yang, Y. H., Paquet, A. & Dudoit, S. R package version 1.12.0 (2006).
34 Tusher, V. G., Tibshirani, R. & Chu, G. Significance analysis of microarrays applied to the ionizing radiation response. *Proc. Natl Acad. Sci. USA* **98,** 5116–5121 (2001).
35 Efron, B. & Tibshirani, R. On testing the significance of sets of genes. *Ann. Appl. Statist.* **1,** 107–129 (2007).

nature cell biology

DOI: 10.1038/ncb2037

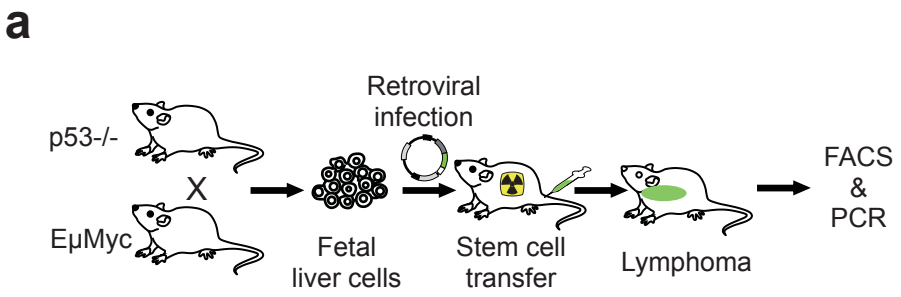

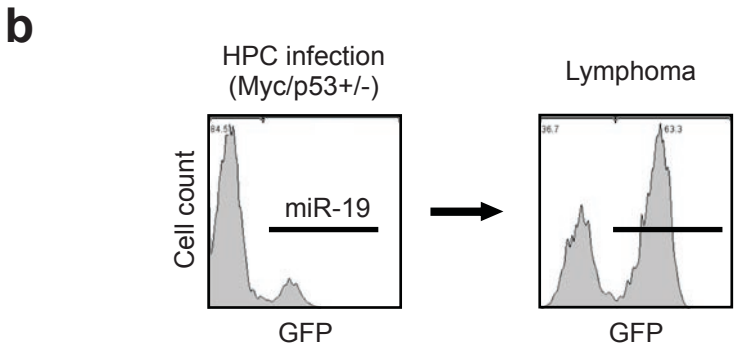

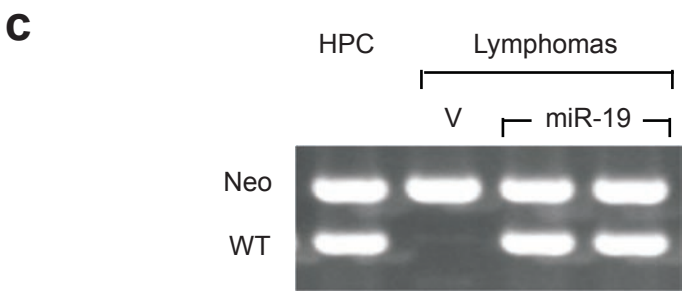

Figure S1 miR-19 cooperates with *c-Myc* and blocks *p53*-dependent apoptosis in *EμMyc* lymphoma. **a)** Schematic of experimental design to generate miR-19-expressing lymphomas derived from *EμMyc/p53+/-* HPCs; **b)** miR-19 expressing HPCs are rapidly enriched during *Myc*-driven lymphomagenesis *in vivo*; **c)** PCR to assess loss of heterozygosity in the *p53* locus in vector and miR-19 expressing lymphomas derived from *EμMyc/p53+/-* HPCs (Neo and Wt indicate the knockout and wild type alleles of *p53*).

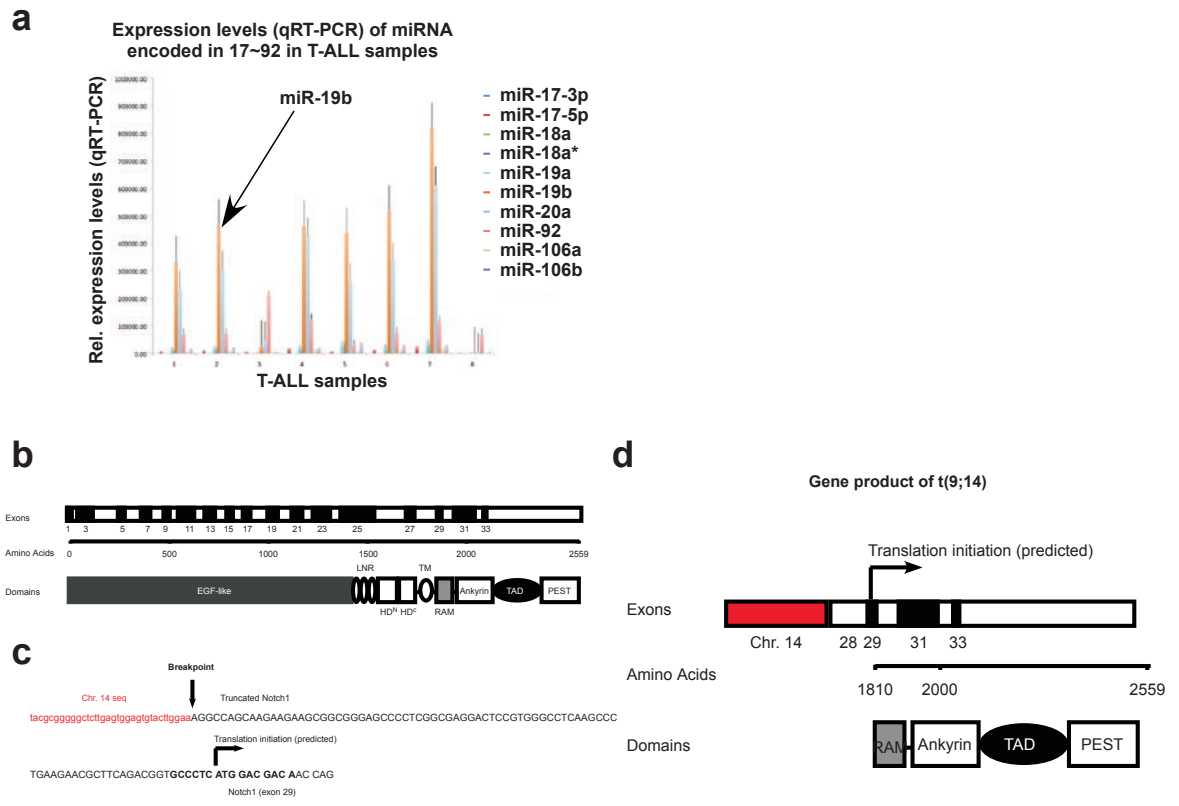

Figure S2 The 17~92 cluster of miRNAs in clinical T-ALL specimens. **a,** qRT-PCR measurement of expression levels of all miRNAs encoded in the 17~92 cluster of miRNAs in a panel of human T- cell acute lymphatic leukaemia, normalized to an endogenous control and shown are mean +/- SEM (n=10); **b**, *NOTCH1* gene structure and protein domains corresponding to the full-length *NOTCH1* transcript; **c,** 5'RACE sequence of *NOTCH1* truncated transcript expressed in leukemic lymphoblasts. The chimeric *NOTCH1*-chromosome 14 sequence encompasses *NOTCH1* sequences distal to the breakpoint located in *NOTCH1* exon 28. The first ATG codon for this mRNA is located in *NOTCH1* exon 29. The sequence corresponding to 5'RACE primer located in *NOTCH1* exon 29 is indicated in bold text; **d**, Structure of the truncated *NOTCH1* mRNA generated by the t(9;14); **e,** Higher resolution of double colour FISH pointing to the existence of a T-ALL oncogene localizing to the 17~92 cluster (same as shown in Figure 2). Analysis using a RB1 probe (green) in 13q14 and genomic clones RP11-97P7 and RP11-980D6 overlapping the 17~92 locus in 13q32 (red). Probe RP11-97P7 shows a split signal with retention of half of the clone in chromosome 13 and the other half mapping to the derivative chromosome 14. Probe RP11-980D6 shows small retention of signal in chromosome 13 and with most of the clone mapping to the derivative chromosome 14.

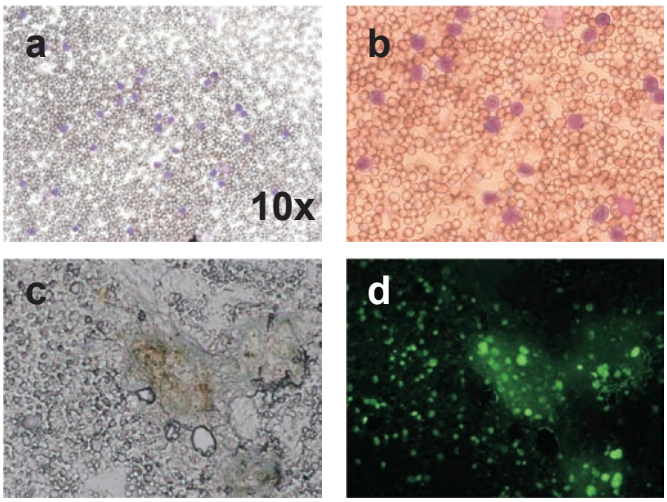

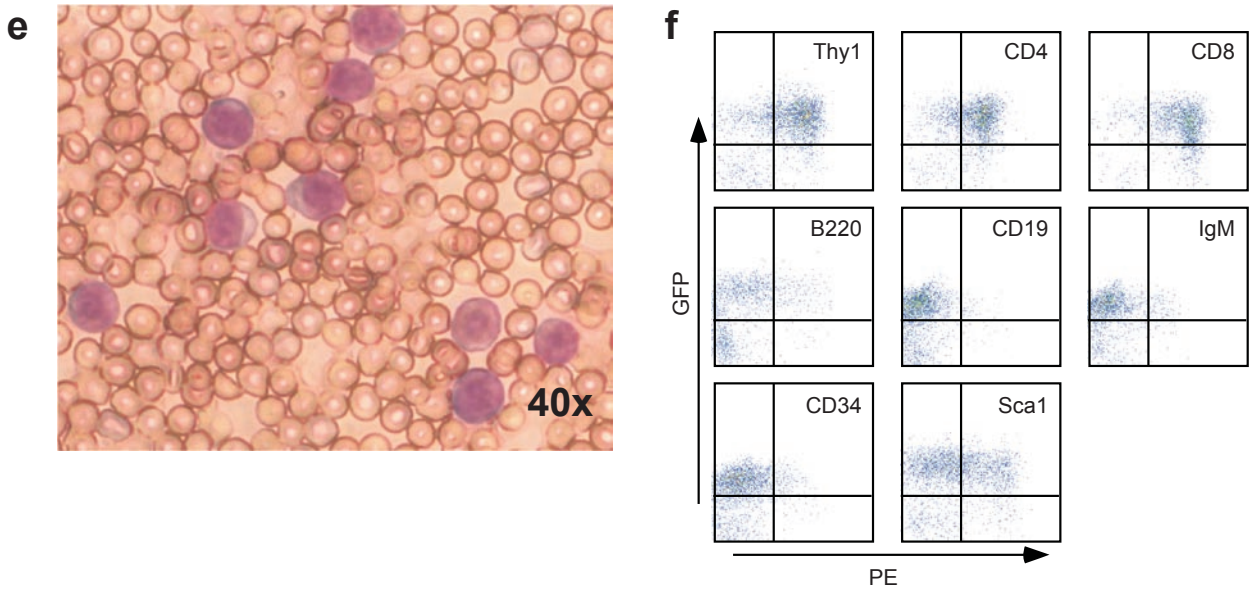

Figure S3 Characterization of miR-19/*Notch-1* induced T-ALL. **a,** Representative microphotograph of a blood film from a leukemic animal at low (10 x) magnification; **b,** high (40 x) magnification of leukemic blasts; **c,** Unstained bone marrow smear and **d,** GFP fluorescence identifies widespread infiltration of marrow by leukemic cells; **e,** higher magnification of lymphoblasts in murine T-ALL; **f,** Immunophenotyping of GFP positive ALL cells using PE-labelled antibodies to the indicated surface markers. Leukaemia arising in *Notch1* transduced HPCs showed the same features (not shown) but a longer latency.

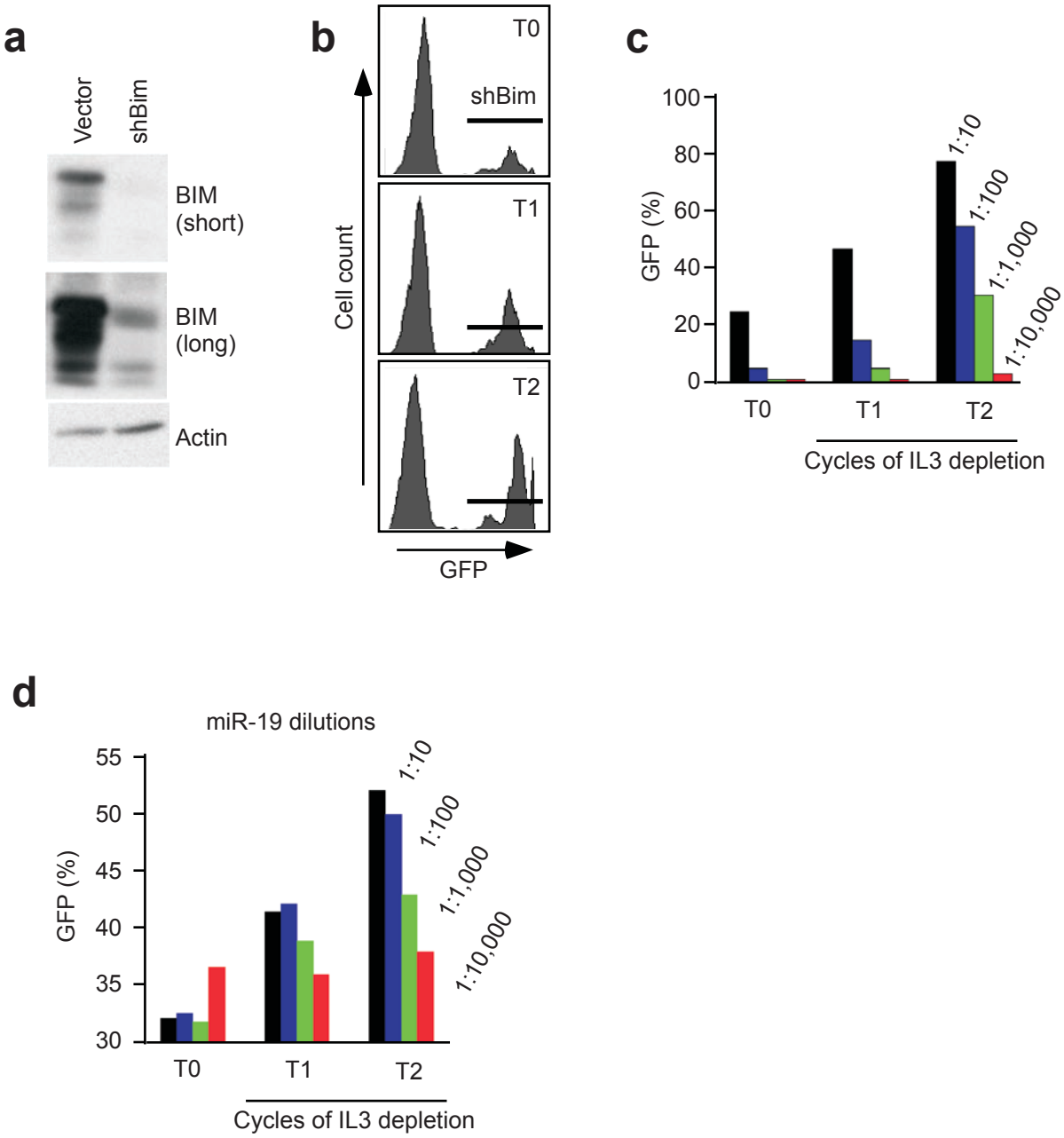

Figure S4 Optimization studies for the shRNA screen. **a,** Immunoblot on FL5-12 cells showing knockdown of BIM/BCl2L11 protein (short and long exposures) by an shRNA against *Bim* compared to vector; **b,** FL5-12 cells expressing the *Bim* shRNA and GFP are enriched in subsequent cycles of IL3 depletion and rescue (T0: untreated, T1: one cycle of IL3 depletion and IL3 rescue, T2: two cycles); **c,** Library reconstruction experiment, the positive control shRNA linked to GFP is diluted with empty vector from 1:10 up to 1:10,000. Enrichment of shRNA and GFP expressing cells is readily detected at dilutions of 1:1,000 and possibly even at 1:10,000; **d**, Library reconstruction experiment using increasing dilutions of miR-19 to characterize in detail miR-19 in the screening assay and conducted as above. Based on these findings the library was constructed to a complexity of ~ 1,000 shRNAs per pool.

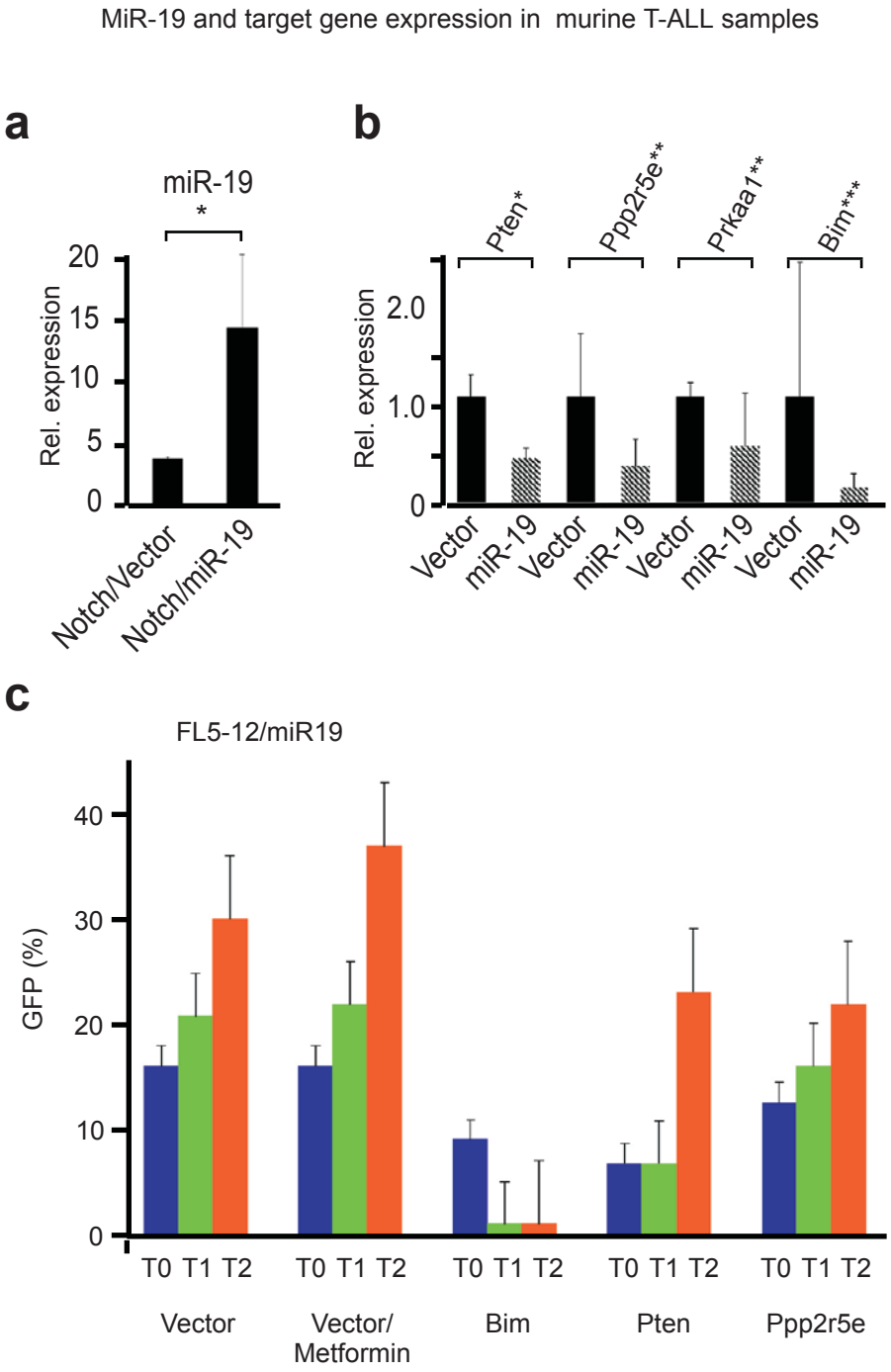

Figure S5 Validation of miR-19 target genes and their functional relevance. **a**, MiR-19 expression is increased in T-ALL derived from HPCs transduced with *Notch1* and miR-19 compared to Notch1 alone (n=3); **b**, The mRNA expression of several target genes is reduced in murine T-ALL driven by *Notch* and miR-19 compared to *Notch* alone (n=3; * $p < 0.05$, and ** $p < 0.1$; *** $p > 0.1$); **c,** Complementation experiments – cDNA expression: Summary of FACS results for enrichment of cells co-expressing miR-19/GFP and the indicated cDNAs or empty vector or treated with 1μM metformin to activate AMP-kinase activity. T0 in presence of IL3, T1 and T2 subsequent time points following IL3 depletion. Standard error (SEM) is indicated, n=3, and p(for all T0 vs. T2) < 0.05). Enforced expression of the pro-apoptotic BIM protein rapidly induced cell death in FL5-12 cells. All other cDNAs or metformin treatment did not abrogate miR-19's protective function.

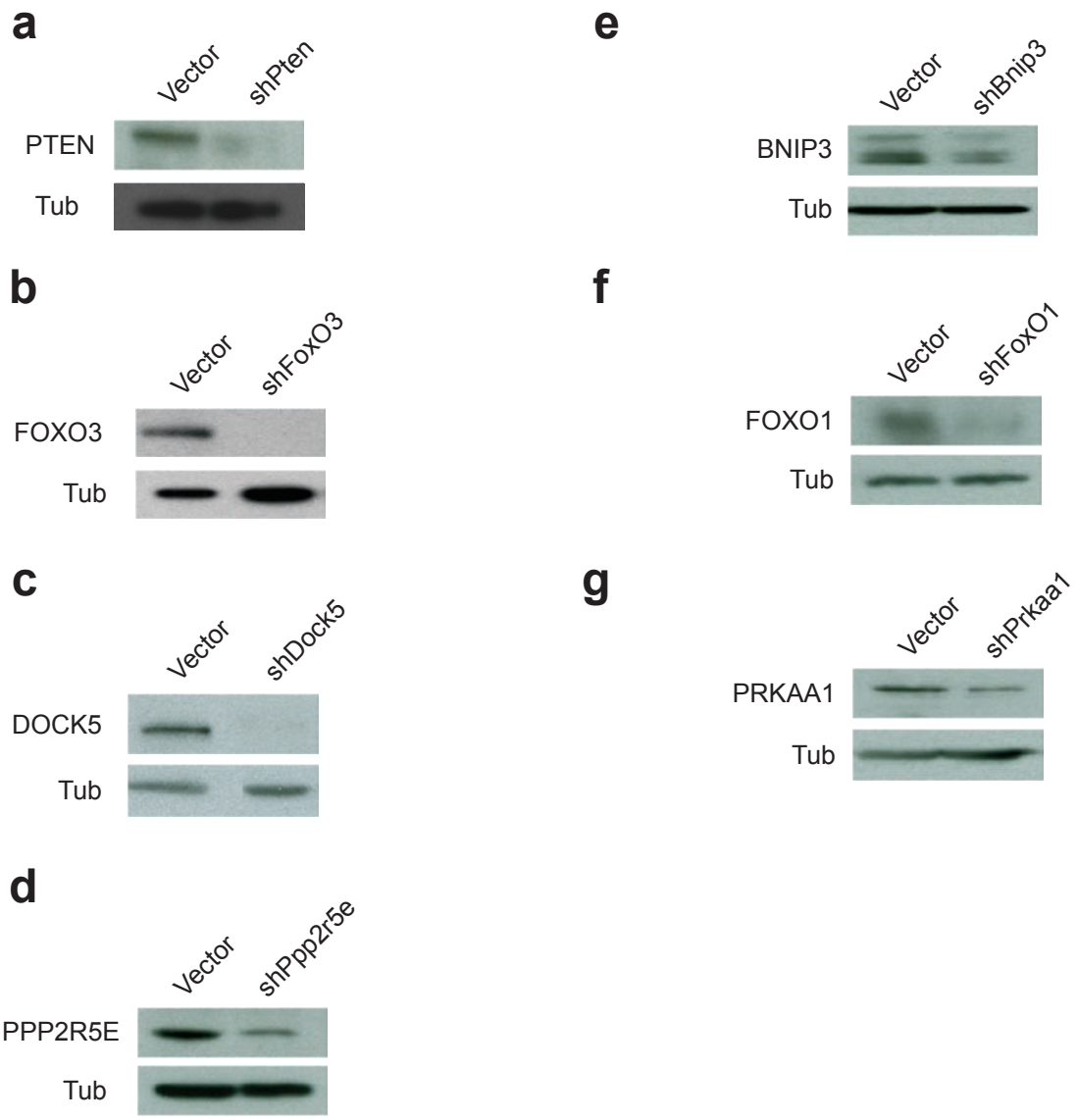

Figure S6 Protein knockdown by shRNA constructs. a-g, Immunoblot on cells transduced with the indicated shRNA constructs and empty vector and probed for the indicated proteins, shown is in each case the most efficient shRNA out of at least 3 shRNA tested.

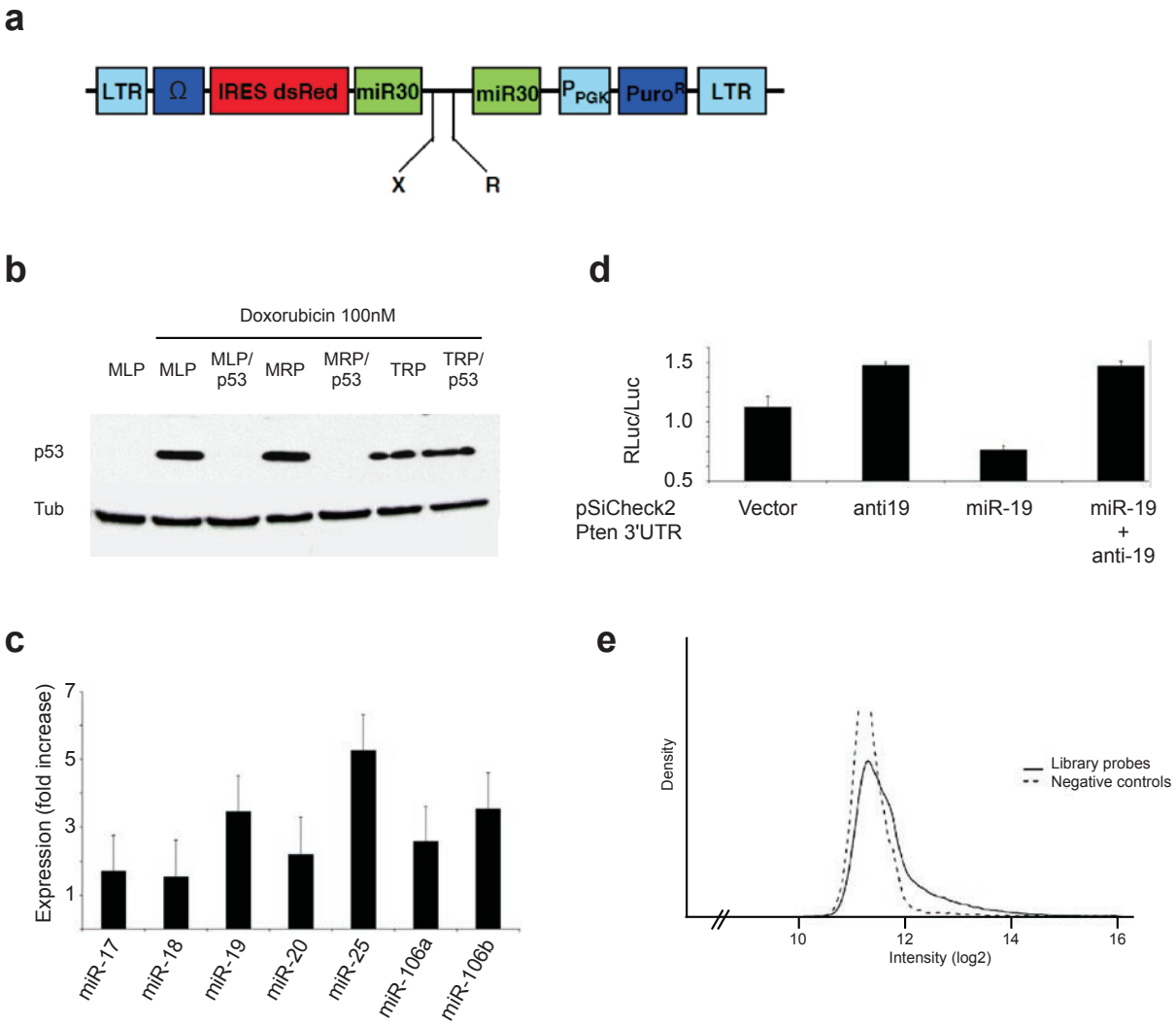

Figure S7 Retroviral shRNA and miRNA vectors. **a,** Diagram of the MSCV-based, MRP retroviral library vector that is used in the shRNA library screen. Note that in validation experiments a GFP expressing version of this construct (MLP) was used for ease of detection; **b,** Immunoblot of lysates from primary fibroblasts treated with doxorubicin to induce p53 or untreated and transduced with the indicated vector constructs with and without the shRNA against *p53*: both MRP and MLP vectors expressing the *p53* shRNA produce efficient protein knockdown; **c,** qRT-PCR analysis of expression of indicated miRNAs in FL5-12 cells infected with MSCV-miR-GFP vectors and FACS sorted; miRNA expression shown as fold increase over vector controls (n=3); **d,** Luciferase reporter assay showing the effectiveness of antagomir-19 in blocking miR-19 mediated inhibition of the Pten-3'UTR (n=3); **e,** Comparison of signal intensity from arrayed half-hairpins that either match shRNAs present in the library (library probes) or negative controls to determine signal/background ratio (see Methods for additional detail).

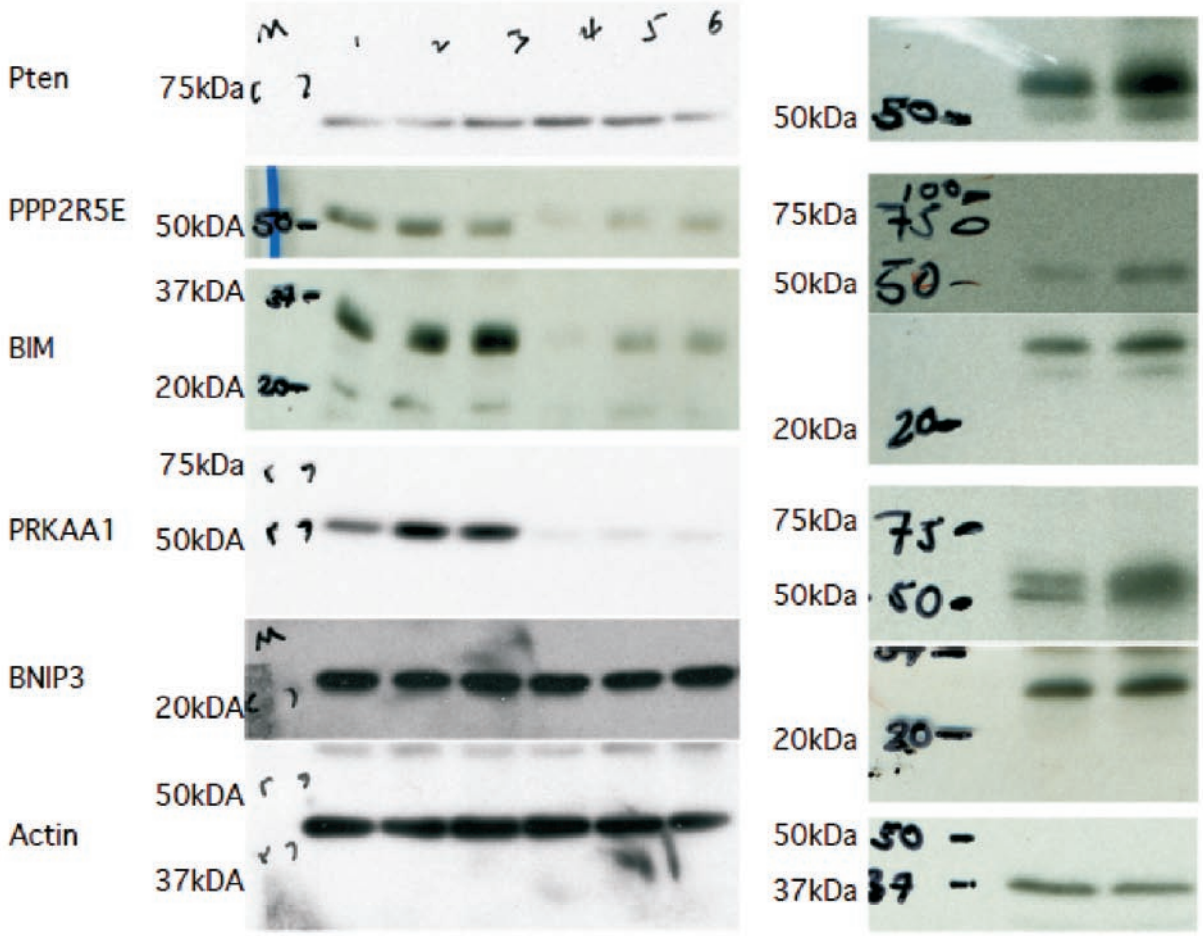

Figure S8 Uncropped scans of immunoblots.

Supplementary Tables

Table S1 qRT-PCR analysis of miR-19 expression in a panel of human lymphatic malignancies and control cells.

Table S2 Surface marker expression in Notch-ICN/Vector and Notch-ICN/miR-19 induced leukaemia.

Table S3 Targetscan prediction of miR-19 targets in the human genome.

Table S4 Targetscan prediction of miR-19 targets in the murine genome.

Table S5 Gene expression analysis of vector and miR-19 expressing FL5-12 cells. Shown are genes whose expression is decreased by ≥ 1SD.

Table S6 Statistical analysis of the shRNA screen results (1): SAM - statistical analysis of microarray data. Shown are the 250 highest scoring shRNAs, individually validated shRNAs are shown in bold print, and the threshold for validation studies is indicated in bright yellow (1.65 fold change, $p < 0.05$).

Table S7 Statistical analysis of the shRNA screen results (2): GSA - Gene set enrichment analysis. Shown are the 250 highest scoring gene sets, gene sets in bold letters individually validated. All gene sets receiving a positive score were validated (except olfactory receptor 481).

Table S8 qRT-PCR analysis of gene expression in vector versus miR-19 and vector versus antagomiR-19 expressing FL5-12 cells (mean +/- SD).

Table S9 Luciferase reporter assay for 3'UTR repression by miR-19 (mean +/- SD).

Table S10 Sequences of shRNA constructs.

Table S11 Primers used to generate 3'UTR reporter constructs.

Table S12 miR-19 binding sites and 3'UTR mutagenesis

Table S13 miR-19 binding sites in the coding sequence of the eight genes identified.